



Semnan University

Mechanics of Advanced Composite Structures

journal homepage: <https://MACS.journals.semnan.ac.ir>

Assessment of RBFs Based Meshfree Method for the Vibration Response of FGM Rectangular Plate Using HSDT Model

M.C. Srivastva, J. Singh *

Department of Mechanical Engineering, MMMUT, Gorakhpur-273010, India

KEYWORDS

Free vibration;
FGM plate;
Meshfree;
RBF.

ABSTRACT

Radial basis functions (RBFs) with modified radial distance are proposed for vibration analysis of functionally graded materials (FGM) rectangular plates. The displacement field with five variables higher-order shear deformation theory (HSDT) is considered. The governing differential equations (GDEs) and boundary conditions are obtained using Hamilton's principle. The governing differential equations formulations are solved via strong-form solutions. The rectangular plates are analyzed in the framework of the RBF-based meshfree method. The novelty of the present modified method is to analyze the square and rectangular plates without changing the shape parameters. Here, the seventeen different RBFs are available in various literature to demonstrate the accuracy and efficiency of the present method in terms of the number of nodes and computational time. The results of several numerical examples have shown that the present modified RBF-based mesh-free method can lead to much more accurate solutions. Computational times of different RBFs are also analyzed.

1. Introduction

Generally, models originating from practical applications in industry and engineering don't have an exact solution, or it is exorbitant to be implemented and actualized. Thus, depending upon the computational calculations, mainly numerical methods such intentions are unavoidable. The most significant achievements for solving governing differential equations in the simulation framework are the finite difference method, finite element method, and finite volume method, which relies on a mesh to construct the local approximation of functions. For more accuracy in these methods, we depend on quality mesh generation, and the time cost is very high. Recently, a novel numerical method known as the Meshfree method has drawn the attention of solving engineering problems by many researchers. The meshfree name method self-defines the method in which no mesh is required and constructs a functional approximation based on scattered points without mesh connectivity. Recently detailed elucidation of various types of meshfree methods can be discussed by Chen et al.

[1]. Meshfree methods formulations are developed under two categories which are known as strong form-based formulations, such as the radial basis collocation method Kansa [2],[3], and weak form-based formulations, such as the radial point interpolation method Wang and Liu [4]. The meshfree method based on the strong form formulation attracts many researchers due to its high accuracy and fast convergence rate, and it is also implemented easily. The time cost is also significantly reduced. In the previous 25 years, the strong form formulation of the meshfree method, which depends on the RBFs, has gotten an alluring response for solving partial differential equations (PDEs). The RBF-based meshfree method is truly meshfree in nature that can directly discretize GDEs of any order, along with their boundary conditions. The foundation thought of RBF interpolation was introduced by Hardy [5] to appraise the scattered data sets. After two decades, Kansa [3] pioneered the concept of solving PDEs utilized by multiquadric RBF. Franke [6] investigated the assessment of RBFs for scattered data interpolation in terms of time,

* Corresponding author. Tel.: +91-9235500565
E-mail address: jsme@mmmmt.ac.in

cost, accuracy, and simplicity of usage. In the recent past, the RBF-based meshfree method on strong form formulation has been successfully adapted to problems of solid mechanics, especially in beams, plates, shells, and panels, and drew attention due to the absence of a mesh in the researcher's community. The meshfree method for the analysis of plates has been previously examined by numerous authors. The nonlinearity of plates on the von Kármán strain assumptions. Van Do and Lee [7] carried out a modified mesh-free RPIM with a new RBF for the nonlinear bending response of the FGM plate using HSDT. Kumar et al [8] investigated the bending analysis of porous bidirectional FGM plates via meshfree methods. Liu and Gu [9] developed a local radial point interpolation method replacing the polynomial basis functions with radial basis functions. Liew et al. [10] introduced a review of the developments of element-free or meshless methods and their applications for the analysis of laminated and FGM structures. Ferreira et al. [11] investigated the buckling and vibration response of laminated plates using the RBF-based meshfree method and FSDT. Rodrigues et al. [12] applied Murakami's zig-zag theory with the RBF-finite-difference collocation method for the buckling, bending, and vibration analysis of composite plates. Zhang et al. [13] studied thermal and mechanical buckling responses of FGM plates using a local Kriging meshfree method. Liew et al. [14] studied the buckling and vibration response of plates by reproducing kernel particle approximate based meshfree method and first-order shear deformation theory (FSDT).

The vibration response of FGM plates necessarily includes the solution of eigenvalue problems. The solution of eigenvalue problems utilizing 3D elasticity theories is challenging to get, especially when the material properties vary using the power law. Thus, 2D assumption-based plate theories are developed and effectively-being utilized for the analysis of plates via analytical and numerical methods. Reddy and Cheng [15] studied 3D asymptotic theory in terms of the transfer matrix to investigate harmonic vibration analysis of the FGM plates. Vel and Batra [16] investigated the free and forced vibration of FGM plates using the power series expansion method. Zenkour [17] considered the effect of rotary inertia on the free vibration response of SS FGM thick plates. The free vibration analysis of the FGM plate using the collocation method was investigated by Ferreira et al. [18]. Uymaz and Aydogdu [19] utilized CPT for the 3D solution of the FGM plate using closed-form formulation. Roque et al. [20] investigated the free vibration of the FGM plate using the RBF-based meshless method. Batra [21] applied the

HSDT model for linearly elastic incompressible FGM plates. Fares et al. [22] introduced a refined ESL theory using the mixed variational approach for the deflection and free vibration analysis of FGM plates. Li et al. [23] studied a 3D elasticity solution for the vibration response of FGM plates using the Ritz method in uniformed, linear, and nonlinear types of temperature distribution. Malekzadeh [24] examined the 3D free vibration of the EFGM plate resting on the foundation, and the material properties vary exponentially through the thickness. Zhao et al. [25] implemented an element-free kp-Ritz technique to investigate the free vibration of FGM plates. FSDT examines transverse shear strain and mesh-free kernel functions used to approximate the 2D displacement fields. Atmane et al. [26] studied the free vibration of elastically supported FGM plate with new HSDT modeling the framework of Navier's method. Talha and Singh [27] examined the bending and vibration response of FGM plates via the FEM method. Giunta et al. [28] utilized the Chebyshev series to expand plate displacements, while the Ritz method determined the natural frequencies. Wu and Chiu [29] carried the RMVT-based meshless collocation and element-free Galerkin technique for the quasi-3D free vibration analysis of FGM plates. Zhu and Liew [30] examined the free vibration analysis of FGM plates using FSDT based on the local Kriging meshless technique. Neves et al. [31] studied the static and free vibration analysis of FGM plates via quasi-3D hyperbolic shear deformation theory with an RBF-based meshless technique. Neves et al. [32] proposed to improve the accuracy by introducing a new sinusoidal HSDT for static bending, buckling, and free vibration response of the FGM. Hosseini-Hashemi e. al. [33] studied the free vibration of thick FGM plates based on exact 3D elasticity theory and closed-form formulation. Xiang and Xing [34] introduced a new FSDT model with two independent variables for the free vibration of a rectangular plate. Chakravarty and Pradhan [35] used the Rayleigh-Ritz method to investigate the free vibration of FGM plates under various boundary conditions. Mahi et al. [36] introduced a new hyperbolic HSDT model to avoid utilizing the shear correction factor, which improved the efficiency of bending and free vibration response of isotropic, functionally graded, sandwich, and laminated composite. Su et al. [37] studied FSDT for the free vibration response of thick laminated FGM plate by using the modified Fourier-Ritz method. Chandra et al. [38] investigated vibration analysis of FGM plates using FSDT and a near-field elemental radiator approach to find the radiated acoustic field. Sekkal et al. [39] examined buckling and free vibration analysis of the FGM plate utilizing a

quasi-3D solution. Shahsavari et al. [40] investigated the free vibration of three types of porosity distribution FGM plate by using quasi-3D hyperbolic theory. Xing et al. [41] implemented multiquadric radial basis functions for the free vibration studies of thin FGM plates via the separation-of-variable method. Zhao et al. [42] utilized a 3D exact solution for free vibration analysis of FGM plates under a porous medium with various boundary conditions. Parida and Mohanty [43] utilized HSDT for the free vibration of a skew FGM plate using a finite element approach.

The objective of this paper is to offer modified radial distance in different RBFs for the free vibration of FG rectangular plate by strong form formulation. To the best of the author's knowledge, the first time the RBF-based meshfree method has been used to analyze the free vibration response of the FG rectangular plate without changing the shape parameters. The influence of the grading index, foundation parameters, span-to-thickness ratio, and plate aspect ratio on the free vibration of rectangular FGM is discussed.

2. Theoretical Formulations

2.1. Material properties and constitutive equations

A porous FG rectangular plate of dimensions length a , breadth b , and thickness h in the Cartesian coordinate system (x - y - z) are shown in Figure 1. The modified power-law homogenization technique with porosity distribution effect for material properties is employed, which is formulated by Zhao et al., [42]

$$E(z) = [E_c - E_m] \left(\frac{2z+h}{2h} \right)^n + E_m - \frac{P}{2} (E_c + E_m) \tag{1}$$

$$\rho(z) = [\rho_c - \rho_m] \left(\frac{2z+h}{2h} \right)^n + \rho_m - \frac{P}{2} (\rho_c + \rho_m)$$

where 'n' is the grading index and 'P' is the porosity volume fraction. E and ρ represent the effective material property Young's modulus and mass density respectively, subscripts m and c represent the metallic and ceramic constituents respectively, P is the porosity fraction ($0 < P < 1$) and $P=0$ means pure FG rectangular plate.

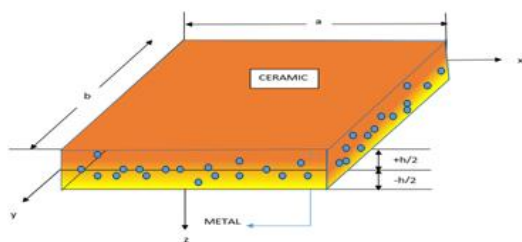


Fig. 1. The geometry of a rectangular FG plate with porosity in the rectangular coordinate system

2.2. Displacement field

The displacement field is a framework as an equivalent single-layer approach with five variables higher order shear deformation theory which can be expressed by Kumar et al. [44].

$$u_x(x, y, \tau) = u_{x0} - z \frac{\partial u_{z0}(x, y, \tau)}{\partial x} + f(z) \chi_x(x, y, \tau)$$

$$u_y(x, y, \tau) = u_{y0} - z \frac{\partial u_{z0}(x, y, \tau)}{\partial y} + f(z) \chi_y(x, y, \tau) \tag{2}$$

$$u_z(x, y, \tau) = u_{z0}$$

where u_x , u_y , u_z , χ_x and χ_y are the five unknown displacement variables and $f(z)$ is the algebraic transverse shear deformation function which is taken from Kumar et al. [44] and τ is the time derivative.

The stress-strain relation using generalized Hook's law with respect to the structural axis system (X - Y - Z) can be expressed as Kumar et al. [44];

$$\begin{Bmatrix} \sigma_{xx} \\ \sigma_{yy} \\ \sigma_{xy} \\ \sigma_{yz} \\ \sigma_{zx} \end{Bmatrix} = \begin{bmatrix} \bar{Q}_{11} & \bar{Q}_{12} & 0 & 0 & 0 \\ \bar{Q}_{12} & \bar{Q}_{22} & 0 & 0 & 0 \\ 0 & 0 & \bar{Q}_{66} & 0 & 0 \\ 0 & 0 & 0 & \bar{Q}_{44} & 0 \\ 0 & 0 & 0 & 0 & \bar{Q}_{55} \end{bmatrix} \begin{Bmatrix} \epsilon_{xx} \\ \epsilon_{yy} \\ \gamma_{xy} \\ \gamma_{yz} \\ \gamma_{zx} \end{Bmatrix} \tag{3}$$

$\bar{Q}_{i,j}$ is plane stress-reduced stiffness and is given below [33].

$$\bar{Q}_{11} = \bar{Q}_{22} = \frac{E(z)}{(1-\nu^2)}, \quad \bar{Q}_{12} = \frac{\nu E(z)}{(1-\nu^2)}, \tag{4}$$

$$\bar{Q}_{44} = \bar{Q}_{55} = \bar{Q}_{66} = \frac{E(z)}{2(1+\nu)}$$

Hamilton's principle is utilized to formulate the GDEs of the FG plate, which is represented as;

$$\int_{t_1}^{t_2} \delta(\text{KE} - \text{UE}) dt = 0 \tag{5}$$

where KE = Kinetic energy, UE = Strain energy,

The kinetic energy of the FG plate can be expressed as.

$$KE = \frac{1}{2} \int_{-\frac{h}{2}}^{\frac{h}{2}} \int_A \rho \left\{ \left(\frac{\partial x 1}{\partial \tau} \right)^2 + \left(\frac{\partial x 2}{\partial \tau} \right)^2 + \left(\frac{\partial x 3}{\partial \tau} \right)^2 \right\} dz dA \tag{6}$$

The strain energy of the FG plate can be expressed as.

$$UE = \frac{1}{2} \int_{-\frac{h}{2}}^{\frac{h}{2}} \int_A (\sigma_{xx} \epsilon_{xx} + \sigma_{yy} \epsilon_{yy} + \sigma_{xy} \gamma_{xy} + \sigma_{yz} \gamma_{yz} + \sigma_{xz} \gamma_{xz}) dz dA \quad (7)$$

Hamilton's principle is used herein to derive the GDEs of the FG plate along with variationally admissible boundary conditions and collecting the coefficients of δu_{x0} , δu_{y0} , δu_{z0} , $\delta \chi_x$, and $\delta \chi_y$, the governing differential equations of the plate are obtained as:

$$\delta u_{x0} : \frac{\partial N_{xx}}{\partial x} + \frac{\partial N_{xy}}{\partial y} = I_0 \frac{\partial^2 u_{x0}}{\partial \tau^2} - I_1 \frac{\partial^3 u_{z0}}{\partial x \partial \tau^2} + I_3 \frac{\partial^2 \chi_x}{\partial \tau^2} \quad (8)$$

$$\delta u_{y0} : \frac{\partial N_{xy}}{\partial x} + \frac{\partial N_{yy}}{\partial y} = I_0 \frac{\partial^2 u_{y0}}{\partial \tau^2} - I_1 \frac{\partial^3 u_{z0}}{\partial y \partial \tau^2} + I_3 \frac{\partial^2 \chi_y}{\partial \tau^2} \quad (9)$$

$$\delta u_{z0} : \frac{\partial^2 M_{xx}}{\partial x^2} + \frac{\partial^2 M_{yy}}{\partial y^2} + 2 \frac{\partial^2 M_{xy}}{\partial x \partial y} = I_0 \frac{\partial^2 u_{z0}}{\partial \tau^2} + I_1 \left(\frac{\partial^3 u_{x0}}{\partial x \partial \tau^2} + \frac{\partial^3 u_{y0}}{\partial y \partial \tau^2} \right) - I_2 \left(\frac{\partial^4 u_{z0}}{\partial x^2 \partial \tau^2} + \frac{\partial^4 u_{z0}}{\partial y^2 \partial \tau^2} \right) + I_4 \left(\frac{\partial^3 \chi_x}{\partial x \partial \tau^2} + \frac{\partial^3 \chi_y}{\partial y \partial \tau^2} \right) \quad (10)$$

$$\delta \chi_x : \frac{\partial O_{xx}}{\partial x} + \frac{\partial O_{xy}}{\partial y} - Q_x^f = I_3 \frac{\partial^2 u_{x0}}{\partial \tau^2} - I_4 \frac{\partial^3 u_{z0}}{\partial x \partial \tau^2} + I_5 \frac{\partial^2 \chi_x}{\partial \tau^2} \quad (11)$$

$$\delta \chi_y : \frac{\partial O_{xy}}{\partial x} + \frac{\partial O_{yy}}{\partial y} - Q_y^f = I_3 \frac{\partial^2 u_{y0}}{\partial \tau^2} - I_4 \frac{\partial^3 u_{z0}}{\partial y \partial \tau^2} + I_5 \frac{\partial^2 \chi_y}{\partial \tau^2} \quad (12)$$

The axial force resultants, the bending moment resultants M_{ij} , the additional moment resultants related to the transverse shear function O_{ij} , and the transverse shear force resultants Q_x^f and Q_y^f are expressed as:

$$\begin{pmatrix} N_{ij} \\ M_{ij} \\ O_{ij} \end{pmatrix} = \int_{-h/2}^{+h/2} \begin{pmatrix} \sigma_{ij} \\ z \sigma_{ij} \\ f(z) \sigma_{ij} \end{pmatrix} dz \quad (13)$$

And,

$$\begin{pmatrix} Q_x^f \\ Q_y^f \end{pmatrix} = \int_{-h/2}^{+h/2} \begin{pmatrix} \sigma_{xz} \\ \sigma_{yz} \end{pmatrix} \left(\frac{\partial f(z)}{\partial z} \right) dz \quad (14)$$

The inertia terms of rectangular FG plate are expressed as:

$$[I_0, I_1, I_2, I_3, I_4, I_5] = \int_{h_1}^{h_2} \rho(z) (1, z, z^2, f(z), zf(z), f^2(z)) dz \quad (15)$$

The GDEs are expressed in terms of displacement components represented as:

$$\begin{pmatrix} A_{11} \frac{\partial^2 x 1_0}{\partial x^2} + A_{66} \frac{\partial^2 x 1_0}{\partial y^2} \\ A_{12} \frac{\partial^2 x 2_0}{\partial x \partial y} + A_{66} \frac{\partial^2 x 2_0}{\partial x \partial y} \end{pmatrix} + \begin{pmatrix} -B_{11} \frac{\partial^3 x 3_0}{\partial x^3} - B_{12} \frac{\partial^3 x 3_0}{\partial x \partial y^2} - 2B_{66} \frac{\partial^3 x 3_0}{\partial x \partial y^2} \end{pmatrix} \quad (16)$$

$$+ \begin{pmatrix} E_{11} \frac{\partial^2 \chi_x}{\partial x^2} + E_{66} \frac{\partial^2 \chi_x}{\partial y^2} \\ E_{12} \frac{\partial^2 \chi_y}{\partial x \partial y} + E_{66} \frac{\partial^2 \chi_y}{\partial x \partial y} \end{pmatrix} = I_0 \frac{\partial^2 x 1_0}{\partial \tau^2} - I_1 \frac{\partial^3 x 3_0}{\partial x \partial \tau^2} + I_3 \frac{\partial^2 \chi_x}{\partial \tau^2}$$

$$\begin{pmatrix} A_{66} \frac{\partial^2 x 1_0}{\partial x \partial y} + A_{12} \frac{\partial^2 x 1_0}{\partial x \partial y} \\ A_{66} \frac{\partial^2 x 2_0}{\partial x^2} + A_{22} \frac{\partial^2 x 2_0}{\partial y^2} \end{pmatrix} + \begin{pmatrix} -2B_{66} \frac{\partial^3 x 3_0}{\partial x^2 \partial y} - B_{12} \frac{\partial^3 x 3_0}{\partial x^2 \partial y} - B_{22} \frac{\partial^3 x 3_0}{\partial y^3} \end{pmatrix} \quad (17)$$

$$+ \begin{pmatrix} (E_{12} + E_{66}) \frac{\partial^2 \chi_x}{\partial x \partial y} \\ +E_{66} \frac{\partial^2 \chi_y}{\partial x^2} + E_{22} \frac{\partial^2 \chi_y}{\partial y^2} \end{pmatrix} = I_0 \frac{\partial^2 x 2_0}{\partial \tau^2} - I_1 \frac{\partial^3 x 3_0}{\partial y \partial \tau^2} + I_3 \frac{\partial^2 \chi_y}{\partial \tau^2}$$

$$\begin{pmatrix} B_{11} \frac{\partial^3 x 1_0}{\partial x^3} + (B_{12} + 2B_{66}) \frac{\partial^3 x 1_0}{\partial x \partial y^2} + B_{22} \frac{\partial^3 x 2_0}{\partial y^3} \end{pmatrix} - \begin{pmatrix} D_{11} \frac{\partial^4 x 3_0}{\partial x^4} + (2D_{12} + 4D_{66}) \frac{\partial^4 x 3_0}{\partial x^2 \partial y^2} + D_{22} \frac{\partial^4 x 3_0}{\partial y^4} \end{pmatrix} \quad (18)$$

$$+ \begin{pmatrix} (F_{12} + 2F_{66}) \frac{\partial^3 \chi_x}{\partial x \partial y^2} + (B_{12} + 2B_{66}) \frac{\partial^3 x 2_0}{\partial x \partial y^2} \\ F_{22} \frac{\partial^3 \chi_y}{\partial y^3} + (F_{12} + 2F_{66}) \frac{\partial^3 \chi_y}{\partial x^2 \partial y} + F_{11} \frac{\partial^3 \chi_x}{\partial x^3} \end{pmatrix}$$

$$= I_0 \frac{\partial^2 x 3_0}{\partial \tau^2} + I_1 \left(\frac{\partial^3 x 1_0}{\partial x \partial \tau^2} + \frac{\partial^3 x 2_0}{\partial y \partial \tau^2} \right) - I_2 \left(\frac{\partial^4 x 3_0}{\partial x^2 \partial \tau^2} + \frac{\partial^4 x 3_0}{\partial y^2 \partial \tau^2} \right) + I_4 \left(\frac{\partial^3 \chi_x}{\partial x \partial \tau^2} + \frac{\partial^3 \chi_y}{\partial y \partial \tau^2} \right)$$

$$\begin{aligned}
 & \left(E_{11} \frac{\partial^2 x 1_0}{\partial x^2} + E_{66} \frac{\partial^2 x 1_0}{\partial y^2} \right) \\
 & + \left(E_{12} \frac{\partial^2 x 2_0}{\partial x \partial y} + E_{66} \frac{\partial^2 x 2_0}{\partial x \partial y} \right) \\
 & + \left(-F_{11} \frac{\partial^3 x 3_0}{\partial x^3} - (F_{12} + 2F_{66}) \frac{\partial^3 x 3_0}{\partial x \partial y^2} \right) \\
 & + \left(H_{11} \frac{\partial^2 \chi_x}{\partial x^2} + H_{66} \frac{\partial^2 \chi_x}{\partial y^2} - A_{55} \chi_x \right) \\
 & + \left((H_{12} + H_{66}) \frac{\partial^2 \chi_y}{\partial x \partial y} + H_{22} \frac{\partial^2 \chi_y}{\partial y^2} \right) \\
 & = I_3 \frac{\partial^2 x 1_0}{\partial \tau^2} - I_4 \frac{\partial^3 x 3_0}{\partial x \partial \tau^2} + I_5 \frac{\partial^2 \chi_x}{\partial \tau^2}
 \end{aligned} \tag{19}$$

$$\begin{aligned}
 & \left(E_{66} \frac{\partial^2 x 1_0}{\partial x \partial y} + E_{12} \frac{\partial^2 x 1_0}{\partial x \partial y} \right) \\
 & + \left(+E_{66} \frac{\partial^2 x 2_0}{\partial x^2} + E_{22} \frac{\partial^2 x 2_0}{\partial y^2} \right) \\
 & + \left(-(F_{12} + F_{66}) \frac{\partial^3 x 3_0}{\partial y \partial x^2} - F_{22} \frac{\partial^3 x 3_0}{\partial y^3} \right) \\
 & + \left(H_{66} \frac{\partial^2 \chi_x}{\partial x \partial y} + H_{12} \frac{\partial^2 \chi_x}{\partial x \partial y} \right) \\
 & + \left(H_{66} \frac{\partial^2 \chi_y}{\partial x^2} + H_{22} \frac{\partial^2 \chi_y}{\partial y^2} - A_{44} \chi_y \right) \\
 & = I_3 \frac{\partial^2 x 2_0}{\partial \tau^2} - I_4 \frac{\partial^3 x 3_0}{\partial y \partial \tau^2} + I_5 \frac{\partial^2 \chi_y}{\partial \tau^2}
 \end{aligned} \tag{20}$$

2.3. Boundary Conditions

The boundary conditions for an arbitrary edge with simply supported (SS) condition is as follows:

$$\begin{aligned}
 & x = 0, \\
 & a : u_y = 0; \chi_y = 0; u_z = 0; M_{xx} = 0; N_{xx} = 0 \\
 & y = 0, \\
 & b : u_x = 0; \chi_x = 0; u_z = 0; M_{yy} = 0; N_{yy} = 0
 \end{aligned} \tag{21}$$

3. Solution Methodology

The importance of RBF-based meshfree methods is that it discretizes the GDEs directly and produce a high rate of convergence with good accuracy. The firm establishment of RBF came to light in the early 1970s, when it was utilized for fitting scattered data [5]. And almost after two decades, Kansa [2][3] used RBF directly to solve partial differential equations that help to initiate

the pillar of new methods by using different types of RBFs.

In the present analysis, we have considered nodes distribution uniformly for a 2-D rectangular domain having IN interior nodes, BN boundary nodes, and N is the total nodes which are the sum of IN and BN which is shown in Singh and Shukla[45]. All computational calculations are carried out in MATLAB with a 2.7 GHz Corei7 processor.

Here, we have considered seventeen types of RBFs that are used in various kinds of computational engineering applications and are listed in Table 1. The considered GDEs with five unknown variables $u_{x0}, u_{y0}, u_{z0}, \chi_x$ and χ_y can be an interpolation in the form of the modified radial distance between nodes. In order to eliminate the singularity, an infinitesimally small value is added for zero radial distance. The radial distance between two nodes is denoted by 'r' and the modification of radial distance between the nodes for rectangular coordinates is done in such a way that the aspect ratio starts changing without changing the shape parameters. The expression used for square plate $r = \|X - X_j\| = \sqrt{(x - x_j)^2 + (y - y_j)^2}$ has been modified as $r = \|X - X_j\| = \sqrt{\left(\frac{x - x_j}{a}\right)^2 + \left(\frac{y - y_j}{b}\right)^2}$ for rectangular plate where a and b are the length and breadth of a rectangular plate.

Table 1 Various types of RBFs used in computation applications.

S.N.	RBF
1	Polynomial, g1 r^k
2	Gaussian quadratic, g2 $e^{(-k^2 r^2)}$
3	Thin Plate Spline, g3 $\log(r)r^{2k}$
4	Wendland's C2, g4 $(1 - kr)^4 (4kr + 1)$
5	Wendland's C4, g5 $(1 - kr)^6 \left((35(kr)^2) + (18kr) + 3 \right)$
6	Wendland's C6, g6 $(1 - kr)^8 \left((32(kr)^3) + (25(kr)^2) + (8kr) + 1 \right)$
7	Hyperbolic secant, g7 $\text{sech}(k\sqrt{r})$
8	Wu-C2, g8 $(1 - kr)^5 \left(8 + 40kr + 48(kr)^2 + 25(kr)^3 + 5(kr)^4 \right)$
9	Wu-C4, g9 $(1 - kr)^6 \left(6 + 36kr + 82(kr)^2 + 72(kr)^3 + 30(kr)^4 + 5(kr)^5 \right)$
10	Hardy's Multiquadric, g10 $\sqrt{(k^2 + r^2)}$

S.N.	RBF
11	Hardy's Inverse Quadric g11 $(k^2 + r^2)^{-1}$
12	Multi-quadratic, g12 $\sqrt{1 + (kr)^2}$
13	Inverse Multi-quadratic, g13 $(\sqrt{1 + (kr)^2})^{-1}$
14	Generalized Inverse Multi-quadratic, g14 $(1 + (kr)^2)^{-2}$
15	Inverse quadratic, g15 $(1 + (kr)^2)^{-1}$
16	Multi-quadratic Shu II, g16 $\sqrt{r^2 + k}$
17	Inverse Multi-quadratics, g17 $(\sqrt{r^2 + k})^{-1}$

'k' is the shape parameter that is responsible for the accurate numerical solution and stability of the method in the computational domain. It is additionally reported that stability and accuracy both simultaneously can't be ensured.

All the five variables of Equation (2) have been discretized from seventeen RBFs for nodes 1: N, as:

$$u_{x0}, u_{y0}, u_{z0}, \chi_x, \chi_y = \sum_{j=1}^N (\alpha_j^{u_{x0}}, \alpha_j^{u_{y0}}, \alpha_j^{u_{z0}}, \alpha_j^{\chi_x}, \alpha_j^{\chi_y}) gi(\|X - X_j\|, k) \quad (22)$$

$$\delta = [\alpha_j^{u_{x0}}, \alpha_j^{u_{y0}}, \alpha_j^{u_{z0}}, \alpha_j^{\chi_x}, \alpha_j^{\chi_y}]^T$$

where, δ is unknown coefficients of unknown variables.

In the eigenvalue problems, the objective is to obtain eigenvalues (λ) and corresponding eigenvectors δ . The eigenvalue problem can be expressed as:

$$\begin{bmatrix} L \\ B \end{bmatrix}_{5N \times 5N} \{\delta\}_{5N \times 1} = \lambda \begin{bmatrix} A \\ 0 \end{bmatrix}_{5N \times 5N} \{\delta\}_{5N \times 1} \quad (23)$$

Equation (23) is solved by standard eigen solvers of computational software to obtain eigenvalues and eigenvectors.

$$\{\delta\} = \left(\begin{bmatrix} [K]_I \\ [K]_B \end{bmatrix} \right)^{-1} \begin{bmatrix} [F]_L \\ 0 \end{bmatrix} \quad (24)$$

$$[K]_I = \quad (25)$$

$$\begin{bmatrix} [K]_{1r}^I(NI,NI) & [K]_{1v}^I(NI,NI) & [K]_{1w}^I(NI,NI) & [K]_{1\phi_x}^I(NI,NI) & [K]_{1\phi_y}^I(NI,NI) \\ [K]_{2r}^I(NI,NI) & [K]_{2v}^I(NI,NI) & [K]_{2w}^I(NI,NI) & [K]_{2\phi_x}^I(NI,NI) & [K]_{2\phi_y}^I(NI,NI) \\ [K]_{3r}^I(NI,NI) & [K]_{3v}^I(NI,NI) & [K]_{3w}^I(NI,NI) & [K]_{3\phi_x}^I(NI,NI) & [K]_{3\phi_y}^I(NI,NI) \\ [K]_{4r}^I(NI,NI) & [K]_{4v}^I(NI,NI) & [K]_{4w}^I(NI,NI) & [K]_{4\phi_x}^I(NI,NI) & [K]_{4\phi_y}^I(NI,NI) \\ [K]_{5r}^I(NI,NI) & [K]_{5v}^I(NI,NI) & [K]_{5w}^I(NI,NI) & [K]_{5\phi_x}^I(NI,NI) & [K]_{5\phi_y}^I(NI,NI) \end{bmatrix}_{(5NI \times 5NI)}$$

$$[K]_B = [O]_{(5 \times NB, 5 \times N)} \quad (26)$$

here, $[K]_I$ represents the stiffness matrix for interior points resulting from LHS of Eq. (25).

The boundary conditions can be discretized in a similar fashion. For example, simply supported boundary condition at the edge $x=0$ is discretized and finally expressed as:

$$[K]_B \{\delta\} = \{O\} \quad (27)$$

where

$$[K]_B = \quad (28)$$

$$\left[[K]_{b,y=0} [K]_{b,x=a} [K]_{b,y=b} [K]_{b,x=0} \right]_{(5 \times NB, 5 \times N)}^T$$

while discretizing the boundary, corner nodes are considered only once.

The unknown coefficients $\{\delta\}$ are calculated from equation (24) obtained, and finally, using equations (22), u_0, v_0, w_0, ϕ_x and ϕ_y at desired locations are obtained. Using equation (2), the displacement components, and using equation (3), the stress components are obtained.

4. Result and Discussions

In the following, we demonstrate the implementation of seventeen types of RBF-based meshfree methods for free vibration response of rectangular FG plate. The stability and performance of the proposed modified RBFs-based meshfree method have been checked by convergence and time study. A simply supported FG rectangular plate is considered throughout the study. Three types of FG rectangular plates, FG1, FG2, and FG3, are considered, and the material property is described in Table 2.

Convergence study

In this section, we examine the impact of the number of nodes on the normalized natural frequency of the rectangular FG1 plate. The plate geometry is defined by uniformly distributed nodes. The results related to the convergence study are explored in Table 3. It is noticed that the present solution obtained by the proposed modified RBFs converged well and is also in good agreement with the result presented in the literature by the 3D HSDT solution of Jin et al. [46]. It can also be noted that all the RBFs produced good results, and the convergence rate is less than 1% after 14x14 nodes. So, based on the convergence study, a 15x15 node is used throughout the study.

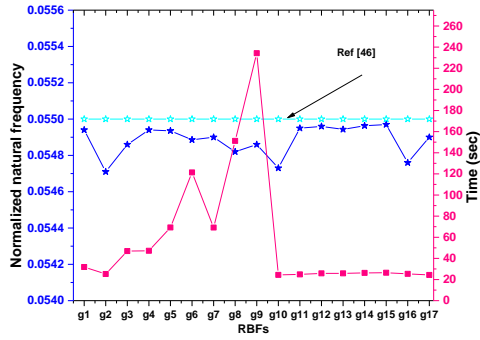


Fig. 2. Comparison study of the natural frequency with the computational speed of different RBF

Table 2 Mechanical properties of metallic and ceramic materials considered.

Types of Functionally graded material		Properties		
		E (GPa)	ρ (kg/m ³)	ν
FG1	Metal (Al)	70	2702	0.3
	(Al2O3)	380	3800	0.3
FG2	(Al)	70	2702	0.3
	(ZrO2)	200	5700	0.3
FG3	(Ti-6Al-4V)	105.7	4429	0.298
	(Aluminum oxide)	320.2	3750	0.26

Table 3. Convergence study of non-dimensional frequency parameters $\bar{\omega} = \omega h \sqrt{\rho_m / E_m}$ of rectangular plates (a/h=10, n=1, b/a=2).

RBFs	Number of nodes						Jin et al., [46]
	11x11	12x12	13x13	14x14	15x15	16x16	
g1	0.05494	0.05498	0.05498	0.05493	0.05494	0.05494	0.055
g2	0.05493	0.05482	0.05475	0.05470	0.05471	0.05469	0.055
g3	0.05524	0.05502	0.05491	0.05488	0.05486	0.05486	0.055
g4	0.05494	0.05498	0.05498	0.05493	0.05494	0.05494	0.055
g5	0.0549	0.0549	0.0549	0.0549	0.0549	0.0549	0.055
g6	0.0550	0.0547	0.0548	0.0548	0.0549	0.0549	0.055
g7	0.05501	0.05493	0.05503	0.05499	0.05490	0.05486	0.055
g8	0.05455	0.05468	0.05476	0.05479	0.05482	0.05483	0.055
g9	0.05505	0.05494	0.05489	0.05487	0.05486	0.05486	0.055
g10	0.05476	0.05478	0.05474	0.05474	0.05473	0.05472	0.055
g11	0.05522	0.05510	0.05504	0.05499	0.05495	0.05493	0.055
g12	0.05554	0.05532	0.05512	0.05503	0.05496	0.05492	0.055
g13	0.05556	0.05532	0.05511	0.05502	0.05494	0.05491	0.055
g14	0.05447	0.05547	0.05515	0.05508	0.05496	0.05494	0.055
g15	0.05572	0.05545	0.05516	0.05507	0.05497	0.05499	0.055
g16	0.05481	0.05480	0.05478	0.05478	0.05476	0.05479	0.055
g17	0.05510	0.05499	0.05496	0.05491	0.05490	0.05491	0.055

Table 4. Comparison of non-dimensional frequency parameter with seventeen RBFs of SS FG2 plate with different span to thickness ratio (a=b = 1, n=0.5).

RBFs	Span-to-thickness ratio					Aver diff %
	5	10	20	50	100	
Ref.[39]	1.6149	1.7504	1.7902	1.8017	1.8034	-----
g1	1.5832	1.7393	1.7837	1.7965	1.7983	0.71
g2	1.5924	1.7424	1.7862	1.7989	1.8008	0.47
g3	1.5826	1.7395	1.7834	1.7959	1.7977	0.73
g4	1.5832	1.7393	1.7837	1.7965	1.7983	0.71
g5	1.5804	1.7389	1.7842	1.7974	1.7993	0.72
g6	1.5818	1.7391	1.7835	1.7963	1.7981	0.73
g7	1.5772	1.7390	1.7849	1.7975	1.8152	0.83
g8	1.5794	1.7373	1.7825	1.7957	1.7976	0.81
g9	1.5818	1.7390	1.7835	1.7963	1.7963	0.75
g10	1.5879	1.7414	1.7849	1.7975	1.7993	0.59
g11	1.5842	1.7414	1.7861	1.7992	1.8011	0.58
g12	1.5846	1.7419	1.7867	1.7997	1.8016	0.55
g13	1.5837	1.7411	1.7859	1.7990	1.8008	0.60
g14	1.5868	1.7426	1.7869	1.7998	1.8016	0.51
g15	1.5853	1.7420	1.7867	1.7997	1.8015	0.55
g16	1.5804	1.7375	1.7822	1.7952	1.7970	0.81
g17	1.5945	1.7397	1.7847	1.7977	1.7996	0.52

Now compare all the RBFs in terms of effectiveness (CPU time) and accuracy, which is shown in Fig. 2. It can be noticed that RBFs g8 and g9 consume more time and RBFs g2, g10, g11, g12, g13, g14, g15, g16, and g17 take less time to execute the computational calculation. RBFs g4, g5, g11, g12, g13, g14 and g15 predict closer results with the 3D HSDT solution of Jin et al., [46]. It can be clearly noticed that RBFs g11, g12, g13, g14, and g15 give closer results to Jin et al. [46] with less time as compared to other RBFs. Table 4 represents the effect of the span-to-thickness ratio for seventeen RBFs. The grading index is taken as 0.5 with a=b. It can be observed that all the RBFs predict less than 1 % average difference and show good agreement with the 3D HSDT result by Sekkal et al. It can also be observed that by increasing span-to-thickness ratios, normalized frequency increases, and after a/h=50, the effect is negligible.

To further examine the effectiveness of the proposed modified RBFs for rectangular FG plate, various parametric study is carried out. Table 5 represents the comparison study of seventeen RBFs with various grading indexes. The span-to-thickness ratio is taken as 10 with an aspect ratio =0.5. It can be seen that all the RBFs predict good results and are in agreement with the existing 3D results by Jin et al. [46]. Results are also compared with 2D results of [47], and it is found that the present results are closer to 3D results, which shows the accuracy of the present solution methodology. It can also be observed that g14 and g15 results are more accurate. The normalized frequency decreases by increasing the grading index.

Figure 3 represents non-dimensional frequency parameter with various porosity index for FG1 rectangular plate with a=20h, n=1 and a=0.5b. It can be noticed that RBFs g4, g6, g7, g8, g9, g11, g12, g13, g14, 15, and g17 predict closer to the HSDT result published by Rezaei et al. [48]. It can also be seen that normalized frequency parameters decrease with an increase in the porosity index. Figure 4 represents the comparison study of seventeen RBFs for rectangular FG plates with various aspect ratios. The grading index is taken as 1 with a span-to-thickness ratio =10. It can be seen that all the RBF results predict good agreement with the existing 3D HSDT solution of Jin et al. [46] and the 2D HSDT result by Thai and Choi [47]. It can be noticed that RBFs g1, g4, g11, g12, g13, g14, and g15 predict closer results as compared to other RBFs, and by increasing the aspect ratio, normalized natural frequency increases.

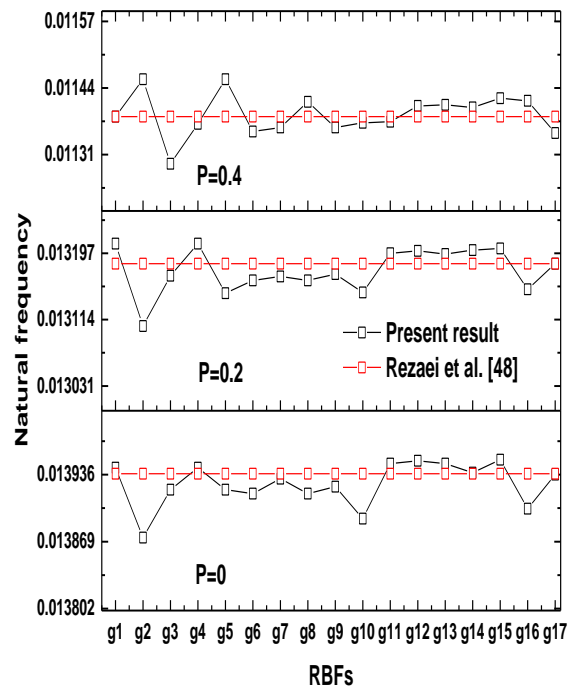


Fig. 3. Comparison study of non-dimensional frequency parameter $\bar{\omega} = \omega h \sqrt{\rho_m / E_m}$ of FG1 rectangular plates with various porosity index (a/h=20, n=1, a/b=0.5)

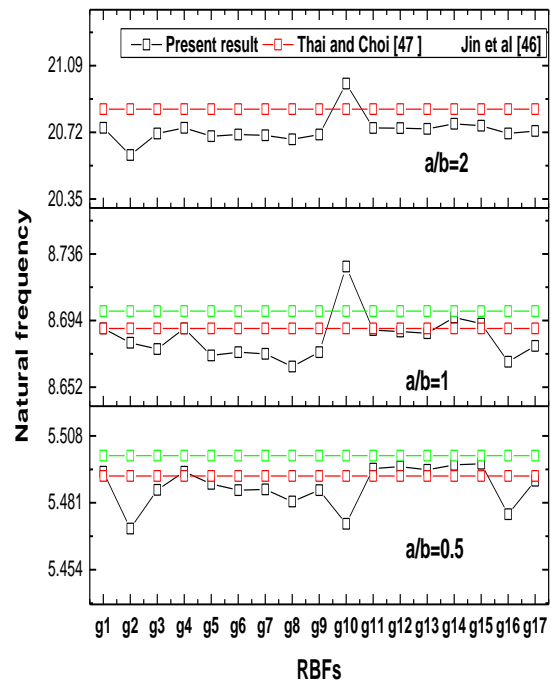


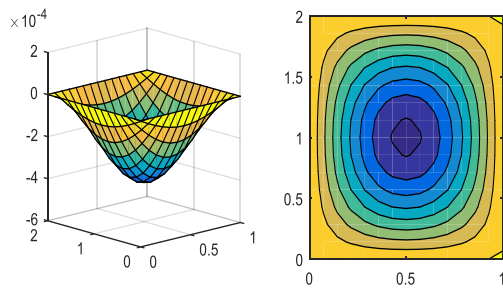
Fig. 4. Comparison study of non-dimensional frequency parameters $\bar{\omega} = \omega a^2 / h \sqrt{\rho_m / E_m}$ of FG1 rectangular plates (a/h=10, n=1)

Table 5. Comparison study of non-dimensional frequency parameter $\bar{\omega} = \frac{\omega a^2}{h} \sqrt{\rho_m/E_m}$ of

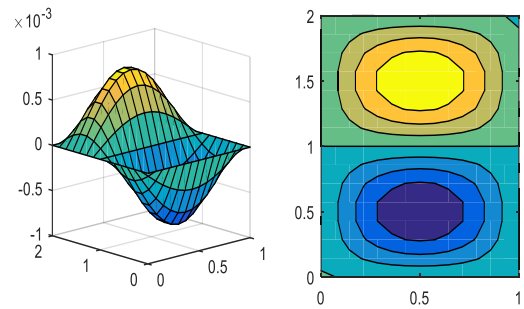
FG1 rectangular plate. (a/h=10, a/b=0.5).

Methods	Grading index				Aver. diff% (2D [47])	Aver. diff% (3D [46])
	0	1	2	5		
Ref.[46] 3D	0.0719	0.0550	0.0499	0.0471	-----	-----
Ref.[47] 2D	0.0717	0.0548	0.0498	0.0470	-----	-----
g1	0.0717	0.0549	0.0499	0.0471	-0.18	0.10
g2	0.0717	0.0547	0.0496	0.0468	0.24	0.51
g3	0.0717	0.0549	0.0498	0.0470	-0.04	0.24
g4	0.0717	0.0549	0.0499	0.0471	-0.18	0.10
g5	0.0718	0.0549	0.0498	0.0469	-0.04	0.24
g6	0.0717	0.0549	0.0498	0.0469	0.00	0.27
g7	0.0716	0.0549	0.0498	0.0470	-0.02	0.25
g8	0.0717	0.0548	0.0498	0.0469	0.03	0.31
g9	0.0717	0.0549	0.0498	0.0470	-0.04	0.24
g10	0.0715	0.0547	0.0497	0.0469	0.19	0.47
g11	0.0718	0.0550	0.0499	0.0470	-0.16	0.11
g12	0.0718	0.0550	0.0499	0.0470	-0.17	0.11
g13	0.0718	0.0549	0.0499	0.0470	-0.16	0.12
g14	0.0718	0.0550	0.0499	0.0471	-0.22	0.05
g15	0.0718	0.0550	0.0499	0.0471	-0.23	0.05
g16	0.0716	0.0548	0.0497	0.0469	0.15	0.42
g17	0.0718	0.0549	0.0498	0.0470	-0.09	0.18

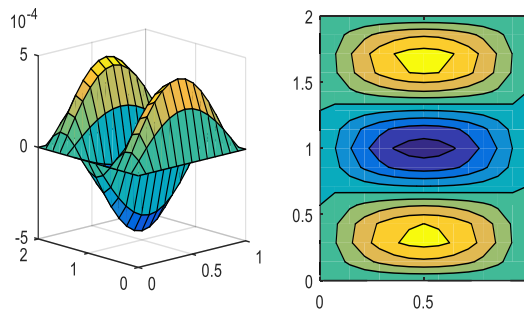
Table 6 shows the results for all 10 modes of non-dimensional frequency parameter $\bar{\omega} = \omega a^2 / h \sqrt{\rho_c / E_c}$ of FGM-3 plate (a=b= 1) for different values of the grading index n = 0, 0.5, 1, 2, 5, 8, 10 and metal with respect to span to thickness ratio. It can be observed that the value of $\bar{\omega}$ increase by increasing the mode. The first three mode shapes and their normalized frequency response $\bar{\omega} = \omega a^2 \sqrt{E_c / \rho_c} / h$ of SS FGM-1 rectangular plate (a/b=0.5, a/h=10, g12, n=1, P=0) are examined and shown in Fig. 5. It seems that the figure with the higher modes plates buckles in different shapes.



Mode 1 = 2.798



Mode 2 = 4.422



Mode 3 = 7.035

Fig. 5. Mode shape of the normalized frequency response of FGM-1 rectangular plate.

Table 6. Effect of grading index 'n' with span-to-thickness ratio on non-dimensional frequency parameter

$$\omega = \omega a^2 / h \sqrt{\rho_c / E_c} \text{ of FGM-3 square plates for mode 10 (g10)}$$

a/h	Modes	Grading Index 'n'							
		0	0.5	1	2	4	8	10	Metal
4	1	4.858	4.051	3.673	3.346	3.115	2.952	2.909	2.587
	2	7.926	6.784	6.176	5.537	5.000	4.628	4.541	4.133
	3	7.926	6.784	6.176	5.537	5.000	4.628	4.541	4.133
	4	9.605	8.107	7.356	6.644	6.090	5.721	5.636	5.086
	5	9.614	8.112	7.361	6.648	6.093	5.724	5.639	5.090
	6	11.154	9.568	8.698	7.690	6.810	6.279	6.181	5.835
	7	11.154	9.583	8.699	7.690	6.810	6.279	6.181	5.843
	8	11.167	9.583	8.699	7.692	6.814	6.284	6.185	5.843
	9	11.167	9.596	8.708	7.692	6.814	6.284	6.185	5.848
	10	11.190	9.596	8.708	7.740	6.864	6.332	6.232	5.848
10	1	5.705	4.722	4.287	3.944	3.735	3.568	3.515	3.056
	2	13.575	11.260	10.217	9.369	8.822	8.406	8.282	7.257
	3	13.576	11.260	10.218	9.370	8.822	8.407	8.282	7.257
	4	19.814	16.978	15.476	13.890	12.542	11.591	11.368	10.334
	5	19.814	16.978	15.476	13.890	12.542	11.591	11.368	10.334
	6	20.734	17.235	15.633	14.294	13.392	12.732	12.546	11.065
	7	25.136	20.923	18.974	17.317	16.176	15.357	15.133	13.399
	8	25.192	20.969	19.016	17.356	16.215	15.394	15.169	13.429
	9	27.975	23.967	21.842	19.599	17.697	16.359	16.045	14.588
	10	31.293	26.104	23.670	21.552	20.051	18.995	18.719	16.657
30	1	5.878	4.858	4.413	4.070	3.868	3.701	3.645	3.153
	2	14.606	12.075	10.966	10.108	9.600	9.184	9.045	7.832
	3	14.607	12.075	10.966	10.108	9.600	9.184	9.045	7.832
	4	23.239	19.216	17.449	16.078	15.258	14.593	14.372	12.457
	5	28.933	23.928	21.725	20.011	18.981	18.150	17.876	15.506
	6	28.971	23.960	21.755	20.039	19.009	18.176	17.902	15.527
	7	37.386	30.928	28.080	25.855	24.508	23.427	23.074	20.032
	8	37.386	30.928	28.080	25.855	24.508	23.427	23.074	20.032
	9	48.730	40.324	36.606	33.686	31.902	30.484	30.026	26.102
	10	48.730	40.324	36.606	33.686	31.902	30.484	30.026	26.102
50	1	5.893	4.870	4.423	4.080	3.878	3.712	3.656	3.161
	2	14.697	12.146	11.031	10.174	9.669	9.254	9.113	7.882
	3	14.697	12.146	11.031	10.174	9.669	9.254	9.113	7.882
	4	23.468	19.397	17.615	16.243	15.434	14.769	14.545	12.585
	5	29.291	24.210	21.985	20.270	19.256	18.426	18.147	15.706
	6	29.326	24.239	22.012	20.295	19.281	18.449	18.169	15.725
	7	37.982	31.398	28.512	26.284	24.963	23.884	23.521	20.365
	8	37.982	31.398	28.512	26.284	24.963	23.884	23.521	20.365
	9	49.737	41.118	37.338	34.411	32.672	31.255	30.781	26.664
	10	49.737	41.118	37.338	34.411	32.672	31.255	30.781	26.664
100	1	5.898	4.874	4.427	4.084	3.883	3.717	3.660	3.164
	2	14.735	12.176	11.059	10.201	9.699	9.283	9.142	7.904
	3	14.735	12.176	11.059	10.201	9.699	9.283	9.142	7.904
	4	23.566	19.474	17.687	16.314	15.510	14.845	14.619	12.640
	5	29.446	24.332	22.097	20.381	19.376	18.546	18.263	15.793
	6	29.478	24.360	22.123	20.406	19.399	18.567	18.285	15.810
	7	38.239	31.600	28.699	26.470	25.162	24.083	23.717	20.509
	8	38.239	31.600	28.699	26.470	25.162	24.083	23.717	20.509
	9	50.176	41.464	37.657	34.729	33.010	31.595	31.114	26.909
	10	50.176	41.465	37.657	34.729	33.010	31.595	31.114	26.909

5. Conclusions

In the present analysis, seventeen radial basis functions have been compared for normalized frequency parameters obtained from five variables HSDT of rectangular FG plate. Hamilton's principle is used to derive a strong form governing differential equations based on the displacement fields. The governing differential equations and boundary conditions are discretized in simultaneous equations using the generalized radial basis function. Modified radial distance-based RBF methods results are in good agreement with various examples available in the literature. The computational speed of RBFs g2, g10, g11, g12, g13, g14, g15, g16, and g17 is good as compared to other RBFs taken here. It also concluded that results produced by g14 g15 are closer to 3D results.

Through the implementation of numerical model results, it is concluded that

- (a) The results obtained by the RBFs have a fast convergence rate (15x15 nodes) with high precision.
- (b) By increasing the grading index, the normalized natural frequency starts decreasing.
- (c) There is an increment in the normalized natural frequency for thick to thin plates, and after $a/h=50$, the effect of the span-to-thickness ratio is constant.
- (d) The normalized frequency decrease with an increase in the porosity index.

Finally, it is up to the research society to sensibly select the RBF that offers more accurate results with less computational cost.

Conflicts of Interest

The author declares that there is no conflict of interest regarding the publication of this manuscript

References

[1] Chen J.-S., Hillman M., Chi S.-W., 2017. Meshfree Methods: Progress Made after 20 Years. *Journal of Engineering Mechanics*, 143(4), pp.04017001.

[2] Kansa E.J., 1990. Multiquadrics-A scattered data approximation scheme with applications to computational fluid dynamics—I surface approximations and partial derivative estimates. *Computers &*

Mathematics with Applications, 19(8), pp.127–145.

- [3] Kansa E.J., 1990. Multiquadrics-A scattered data approximation scheme with applications to computational fluid dynamics—II solutions to parabolic, hyperbolic and elliptic partial differential equations. *Computers & Mathematics with Applications*, 19(8), pp.147–161.
- [4] Wang J.G., Liu G.R., 2002. A point interpolation meshless method based on radial basis functions. *International Journal for Numerical Methods in Engineering*, 54(11), pp.1623–1648.
- [5] Hardy R.L., 1971. Multiquadric equations of topography and other irregular surfaces. *Journal of Geophysical Research*, (1896-1977) 76(8), pp.1905–1915.
- [6] Franke R., 1982. Scattered data interpolation: tests of some methods. *Mathematics of Computation*, 38(157), pp.181–200.
- [7] Van Do V. N., Lee C.-H., 2018. Nonlinear analyses of FGM plates in bending by using a modified radial point interpolation mesh-free method. *Applied Mathematical Modelling*, 57, pp.1–20.
- [8] Kumar R., Singh B. N., Singh J., and Singh J., 2022. Meshfree approach for flexure analysis of bidirectional porous FG plate subjected to I, L, and T types of transverse loading. *Aerospace Science and Technology*, 129, p. 107824
- [9] Liu G. R., Gu Y. T., 2001. A Local Radial Point Interpolation Method (LRPIM) for free vibration analysis of 2-D solids. *Journal of Sound and Vibration*, 246(1), pp. 29–46.
- [10] Lie K. M., Zhao X., Ferreira A. J. M., 2011. A review of meshless methods for laminated and functionally graded plates and shells. *Composite Structures*, 93(8), pp. 2031–2041.
- [11] Ferreira A. J. M., Roque C. M. C., Neves A. M. A., Jorge R. M. N., Soares C. M. M., Liew K. M., 2011. Buckling and vibration analysis of isotropic and laminated plates by radial basis functions. *Composites Part B: Engineering*, 42(3) pp. 592–606.

- [12] Rodrigues J. D., Roque C. M. C., Ferreira A. J. M., Carrera E., and Cinefra M., 2011. Radial basis functions–finite differences collocation and a Unified Formulation for bending, vibration and buckling analysis of laminated plates, according to Murakami's zig-zag theory. *Composite Structures*, 93(7), pp. 1613–1620.
- [13] Zhang L. W., Zhu P., Liew K. M., 2014. Thermal buckling of functionally graded plates using a local Kriging meshless method. *Composite Structures*,108, pp. 472–492,
- [14] Liew K. M., Wang J., Ng T. Y., and Tan M. J., 2004. Free vibration and buckling analyses of shear-deformable plates based on FSDT meshfree method. *Journal of Sound and Vibration*, 276(3), pp. 997–1017.
- [15] Reddy J. N., Cheng Z.-Q., 2003. Frequency of Functionally Graded Plates with Three-Dimensional Asymptotic Approach. *Journal of Engineering Mechanics*,129(8), pp. 896–900.
- [16] Vel S. S. and Batra R. C., 2004. Three-dimensional exact solution for the vibration of functionally graded rectangular plates. *Journal of Sound and Vibration*,272(3), pp. 703–730.
- [17] Zenkour A. M., 2005. On vibration of functionally graded plates according to a refined trigonometricplate theory. *International Journal of Structural Stability and Dynamics*, 05(02), pp. 279–297.
- [18] Ferreira A. J. M., Batra R. C., Roque C. M. C., Qian L. F., Jorge R. M. N., 2006. Natural frequencies of functionally graded plates by a meshless method. *Composite Structures*, 75(1), pp. 593–600.
- [19] Uymaz B. and Aydogdu M., 2007. Three-Dimensional Vibration Analyses of Functionally Graded Plates under Various Boundary Conditions. *Journal of Reinforced Plastics and Composites*,26(18), pp. 1847–1863.
- [20] Roque C. M. C., Ferreira A. J. M., and Jorge R. M. N., 2007. A radial basis function approach for the free vibration analysis of functionally graded plates using a refined theory. *Journal of Sound and Vibration*,300(09), pp. 1048–1070.
- [21] Batra R. C., 2007. Higher-order shear and normal deformable theory for functionally graded incompressible linear elastic plates. *Thin-Walled Structures*,45(12), pp. 974–982.
- [22] Fares M. E., Elmarghany M. Kh., Atta D., 2009. An efficient and simple refined theory for bending and vibration of functionally graded plates. *Composite Structures*,91(3), pp. 296–305.
- [23] Li Q., Iu V. P., Kou K. P., 2009. Three-dimensional vibration analysis of functionally graded material plates in thermal environment. *Journal of Sound and Vibration*.324(3), pp. 733–750.
- [24] Malekzadeh P., 2009. Three-dimensional free vibration analysis of thick functionally graded plates on elastic foundations. *Composite Structures*,89(3), pp. 367–373.
- [25] Zhao X., Lee Y. Y., Liew K. M., 2009. Free vibration analysis of functionally graded plates using the element-free kp-Ritz method. *Journal of Sound and Vibration*,319(3), pp. 918–939.
- [26] Atmane H. A., Tounsi A., Mechab I., Bedia E. A. A., 2010. Free vibration analysis of functionally graded plates resting on Winkler–Pasternak elastic foundations using a new shear deformation theory. *International Journal of Mechanics and Materials in Design*, 6(2), pp. 113–121.
- [27] Talha M. and Singh B. N., 2010. Static response and free vibration analysis of FGM plates using higher order shear deformation theory. *Applied Mathematical Modelling*, 34(12), pp. 3991–4011.
- [28] Giunta G., Crisafulli D., Belouettar S., Carrera E., 2011. Hierarchical theories for the free vibration analysis of functionally graded beams. *Composite Structures*, 94(01), pp. 68–74.
- [29] Wu C.-P., Chiu K.-H., 2011. RMVT-based meshless collocation and element-free Galerkin methods for the quasi-3D free vibration analysis of multilayered composite and FGM plates. *Composite Structures*, 93(5), pp. 1433–1448.
- [30] Zhu P. and Liew K. M., 2011. Free vibration analysis of moderately thick functionally graded plates by local Kriging meshless

- method. *Composite Structures*,93(11), pp. 2925–2944.
- [31] Neves A. M. A., et al., 2012. A quasi-3D hyperbolic shear deformation theory for the static and free vibration analysis of functionally graded plates. *Composite Structures*, 94(5), pp. 1814–1825.
- [32] Thai H.-T. and Vo T. P., 2013. A new sinusoidal shear deformation theory for bending, buckling, and vibration of functionally graded plates. *Applied Mathematical Modelling*, 37(5), pp. 3269–3281.
- [33] Hosseini-Hashemi Sh., Salehipour H., Atashipour S. R., Sburlati R., 2013. On the exact in-plane and out-of-plane free vibration analysis of thick functionally graded rectangular plates: Explicit 3-D elasticity solutions. *Composites Part B: Engineering*, 46, pp. 108–115.
- [34] Xiang W. and Xing Y., 2014. A New First-Order Shear Deformation Theory for Free Vibrations of Rectangular Plate. *International Journal of Applied Mechanics*, 07(01), pp. 1550008.
- [35] Chakraverty S., Pradhan K. K., 2014. Free vibration of functionally graded thin rectangular plates resting on winkler elastic foundation with general boundary conditions using rayleigh–ritz method. *International of Journal Applied Mechanics*, 06(04), pp. 1450043.
- [36] Mahi A., Adda Bedia E. A., Tounsi A., 2015. A new hyperbolic shear deformation theory for bending and free vibration analysis of isotropic, functionally graded, sandwich and laminated composite plates. *Applied Mathematical Modelling*, 39(9), pp. 2489–2508.
- [37] Su Z., Jin G., Wang X., Miao X., 2015. Modified Fourier–Ritz Approximation for the Free Vibration Analysis of Laminated Functionally Graded Plates with Elastic Restraints. *International Journal of Applied Mechanics*, 07(05), pp. 1550073.
- [38] Chandra N., Raja S., Gopal K. V. N., 2015. A Comprehensive Analysis on the Structural–Acoustic Aspects of Various Functionally Graded Plates. *International Journal of Applied Mechanics*, 07(05), pp. 1550072.
- [39] Sekkal M., Fahsi B., Tounsi A., Mahmoud S. R., 2017. A new quasi-3D HSDT for buckling and vibration of FG plate. *Structural engineering and mechanics: An international journal*,64(6), pp. 737–749.
- [40] Shahsavari D., Shahsavari M., Li L., and Karami B., 2018. A novel quasi-3D hyperbolic theory for free vibration of FG plates with porosities resting on Winkler/Pasternak/Kerr foundation. *Aerospace Science and Technology*, 72, pp. 134–149.
- [41] Xing Y. F., Wang Z. K., Xu T. F., 2018. Closed-form Analytical Solutions for Free Vibration of Rectangular Functionally Graded Thin Plates in Thermal Environment," *International Journal of Applied Mechanics*, 10(03), pp. 1850025.
- [42] Zhao J., Choe K., Xie F., Wang A., Shuai C., Wang Q., 2018. Three-dimensional exact solution for vibration analysis of thick functionally graded porous (FGP) rectangular plates with arbitrary boundary conditions. *Composites Part B: Engineering*,155, pp. 369–381.
- [43] Parida S. and Mohanty S. C., 2018. Free Vibration Analysis of Functionally Graded Skew Plate in Thermal Environment Using Higher Order Theory. *International Journal of Applied Mechanics*, 10(01), pp. 1850007.
- [44] Kumar R., Lal A., Singh B. N., Singh J.,2019. New transverse shear deformation theory for bending analysis of FGM plate under patch load. *Composite Structures*,208, pp. 91–100.
- [45] Singh J., Shukla K. K., 2012. Nonlinear flexural analysis of laminated composite plates using RBF based meshless method. *Composite Structures*, vol. 94(5), pp. 1714–1720.
- [46] Jin G., Su Z., Shi S., Ye T., Gao S., 2014. Three-dimensional exact solution for the free vibration of arbitrarily thick functionally graded rectangular plates with general boundary conditions. *Composite Structures*,108, pp. 565–577.
- [47] Thai H.-T. and Choi D.-H., 2012. A refined shear deformation theory for free vibration of functionally graded plates on elastic foundation. *Composites Part B: Engineering*, 43(5), pp. 2335–2347.

- [48] Rezaei A. S., Saidi A. R., Abrishamdari M., Mohammadi M. H. P., 2017. Natural frequencies of functionally graded plates with porosities via a simple four variable plate theory: An analytical approach. *Thin-Walled Structures*,120, pp. 366–377.